Supporting Information

Two-dimensional Janus perovskite oxynitrides as active photocatalysts for overall water splitting with ferroelectric modulation

*Zhichao Yu[1], Bowen Li[1], Haoyun Bai[1], Hui Pan[1,2]**

[1] Institute of Applied Physics and Materials Engineering, University of Macau, Macao SAR 999708, P. R. China

[2] Department of Physics and Chemistry, Faculty of Science and Technology, University of Macau, Macao SAR 999078, P. R. China

*E-mail: huipan@um.edu.mo

Table S1. In-plane elastic constants of $BaTaNO_2$-1, $BaNbNO_2$-1 and $BaVNO_2$-1(kBar)

	C_{11}	C_{12}	C_{22}	C_{66}
$BaTaNO_2$-1	671	213	671	265
$BaNbNO_2$-1	596	183	596	254
$BaVNO_2$-1	131	111	386	161

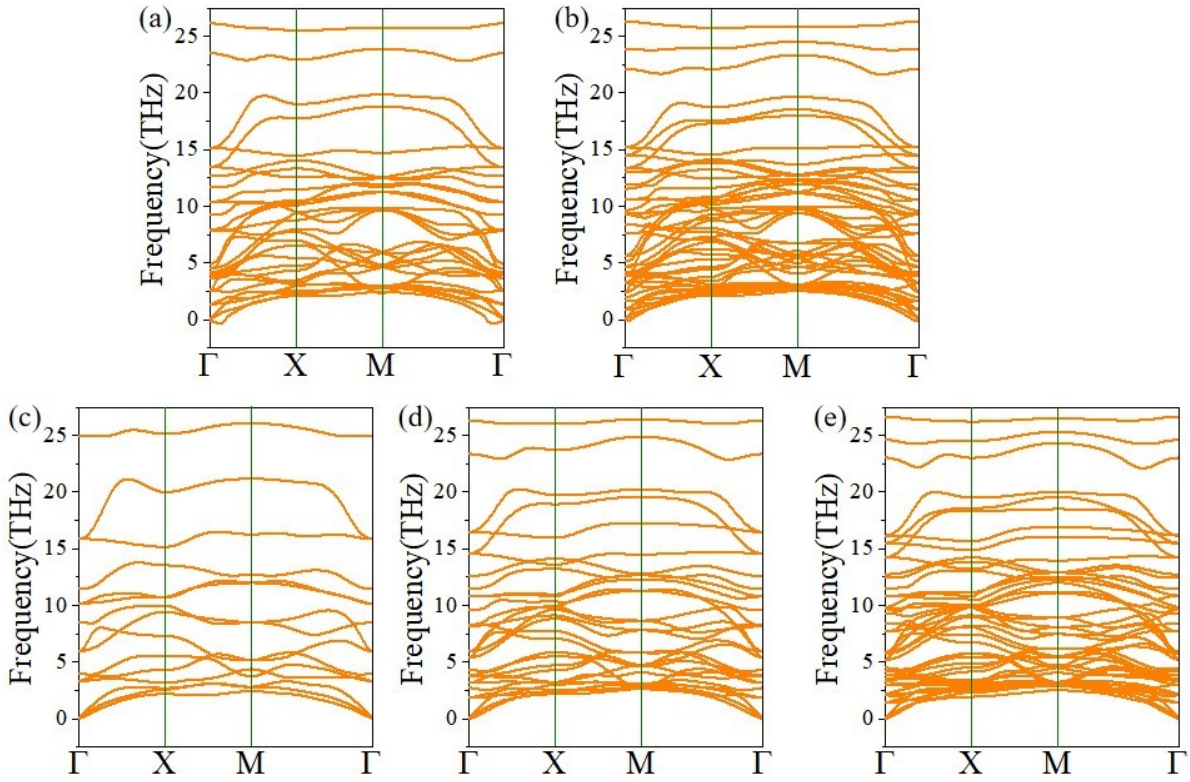

Figure S1: Phonon dispersions of (a) $BaNbNO_2$-2, (b) $BaNbNO_2$-3, (c) $BaTaNO_2$-1, (d) $BaTaNO_2$-2, and (e) $BaTaNO_2$-3.

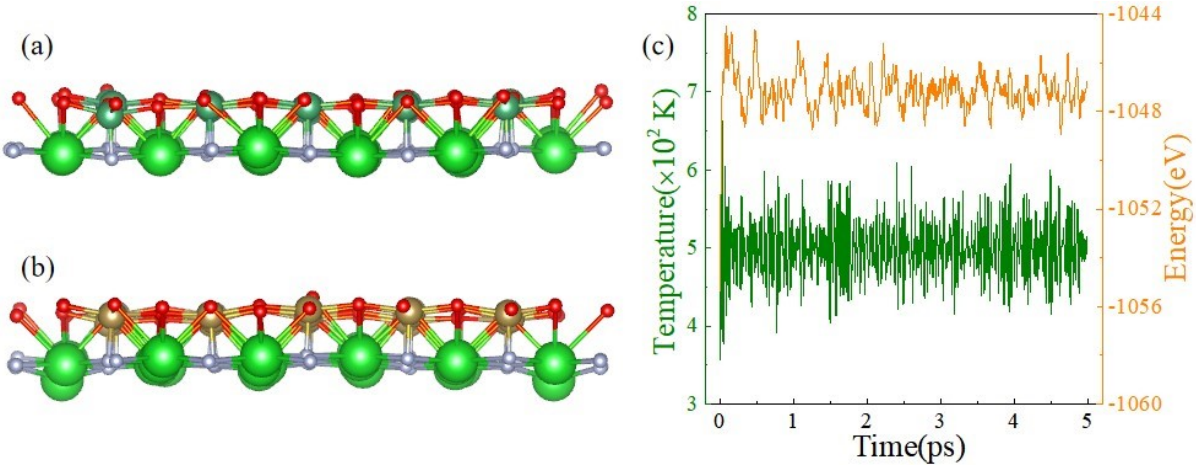

Figure S2: Structure of (a) $BaNbNO_2$-1 and (b) $BaTaNO_2$-1 after AIMD for 5 ps. (c) Total energy (orange) and temperature (olive) of $BaTaNO_2$-1 as a function of time during AIMD.

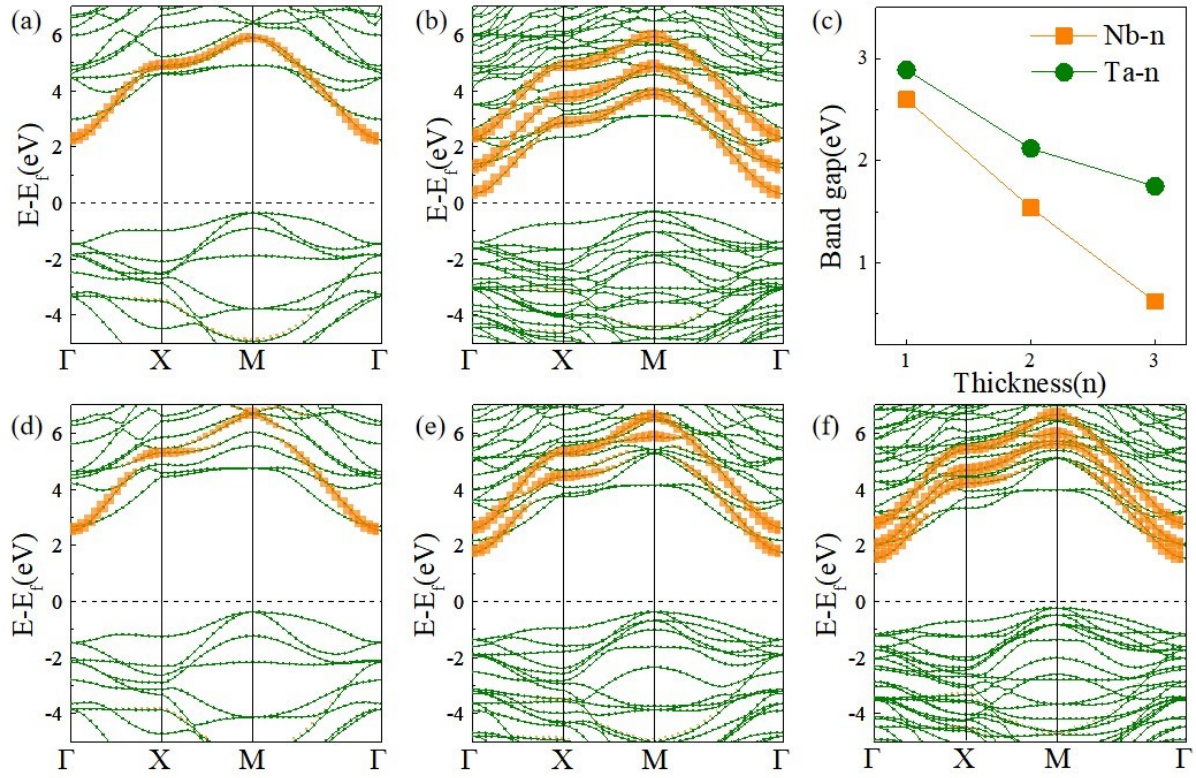

Figure S3: Band structures (olive) and projected band structures (orange) of Nb/Ta-d_{xy} orbitals of (a) $BaNbNO_2$-1, (b) $BaNbNO_2$-3, (d) $BaTaNO_2$-1, (e) $BaTaNO_2$-2, and (f) $BaTaNO_2$-3. (c) Relations between band gap and thickness of $BaXNO_2$-n (X = Nb, Ta).

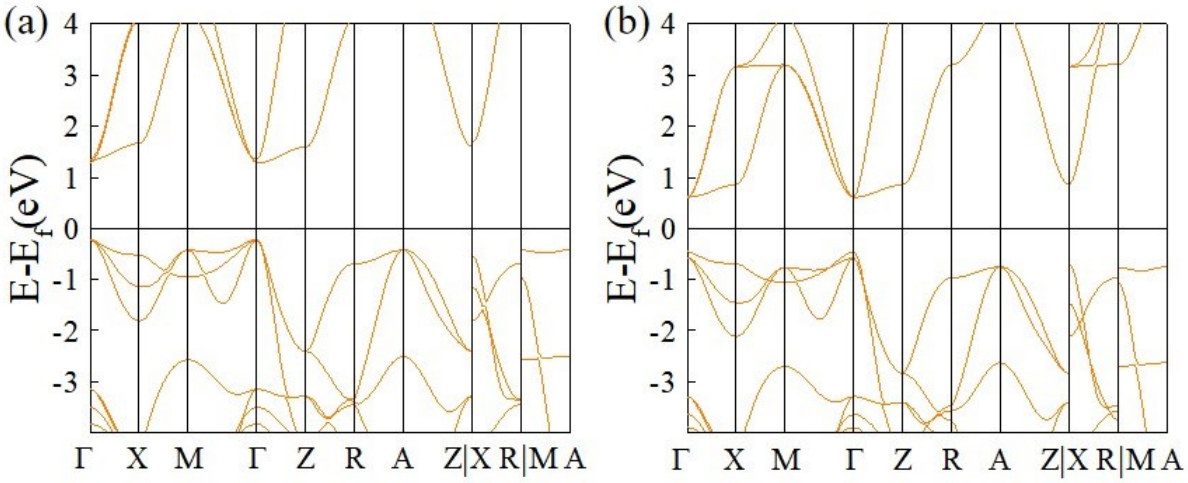

Figure S4: Band structures of (a) $BaTaNO_2$ and (b) $BaNbNO_2$.

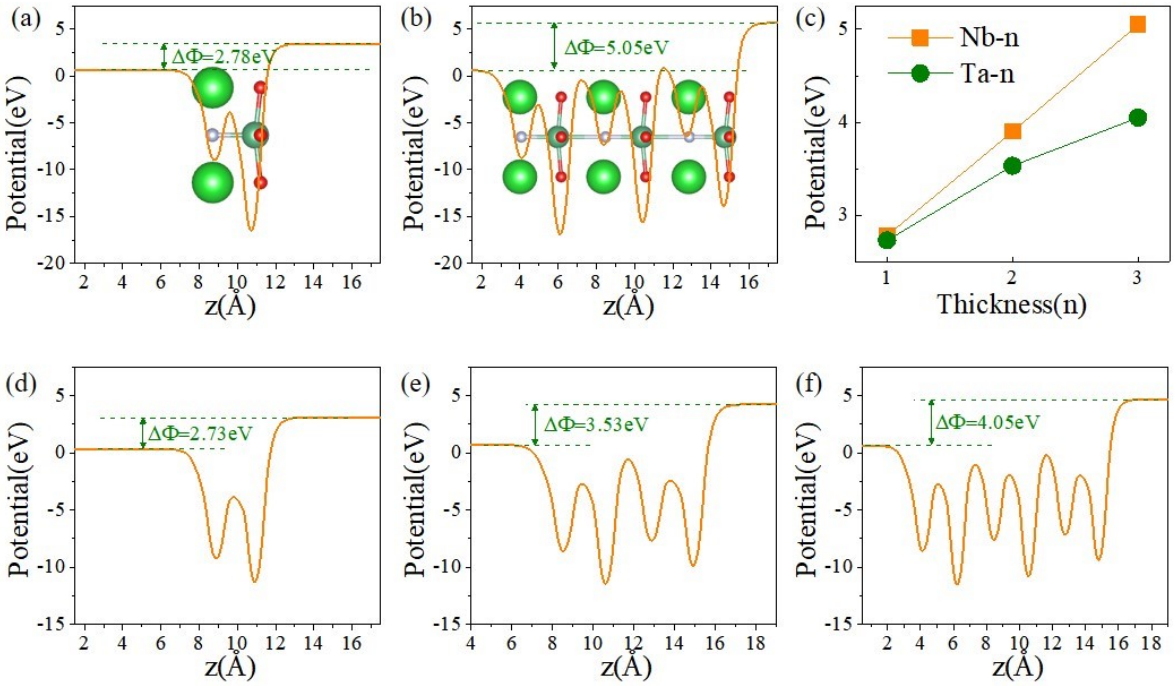

Figure S5: Electrostatic potentials of (a) $BaNbNO_2$-1, (b) $BaNbNO_2$-3, (d) $BaTaNO_2$-1, (e) $BaTaNO_2$-2, and (f) $BaTaNO_2$-3 along the z direction. (c) Relation between electrostatic potential and thickness of $BaXNO_2$-n (X = Nb, Ta).

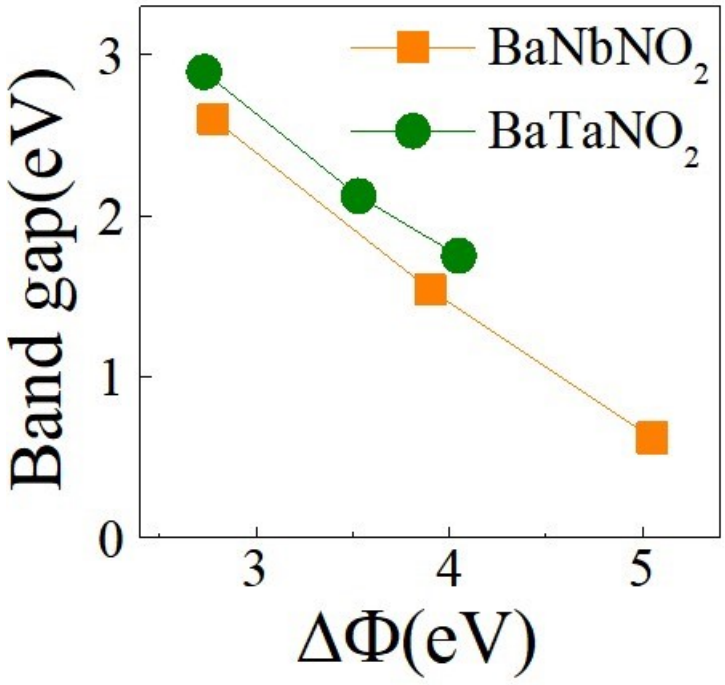

Figure S6: Band gap of $BaXNO_2$ (X = Nb, Ta) as a function of ΔΦ.

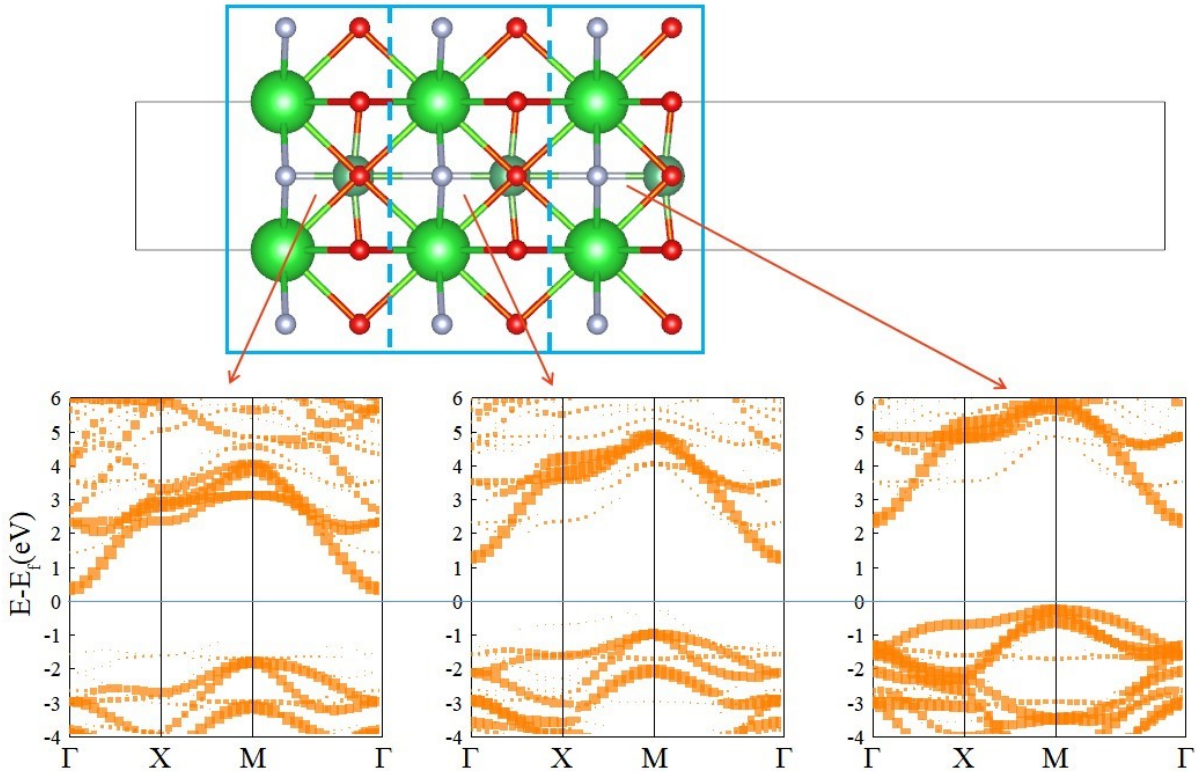

Figure S7: Layer-dependent projected band structure of $BaNbNO_2$-3. The small gap of $BaNbNO_2$-3 comes from the conduction band of bottom layer which constitutes the final CBM of $BaNbNO_2$-3 and the valence band of top layer which constitutes the final VBM of $BaNbNO_2$-3 locate close to each other. The shapes of the layer-dependent band vary a little which is as expected, given interlayer influence should be weak. The gaps of each layer also keep almost same. The only difference lies on the relative energy levels and this trend is easy to understand given its built-in electric field and electrostatic potential difference.

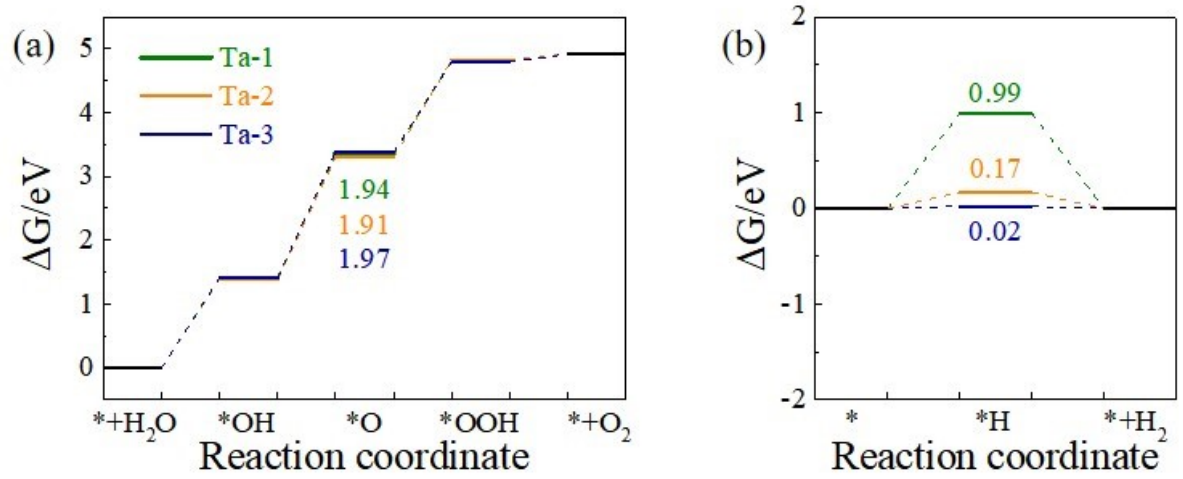

Figure S8: Free energy diagrams of (a) OER and (b) HER for $BaTaNO_2$-1 (olive), $BaTaNO_2$-2 (orange), and $BaTaNO_2$-3 (royal).

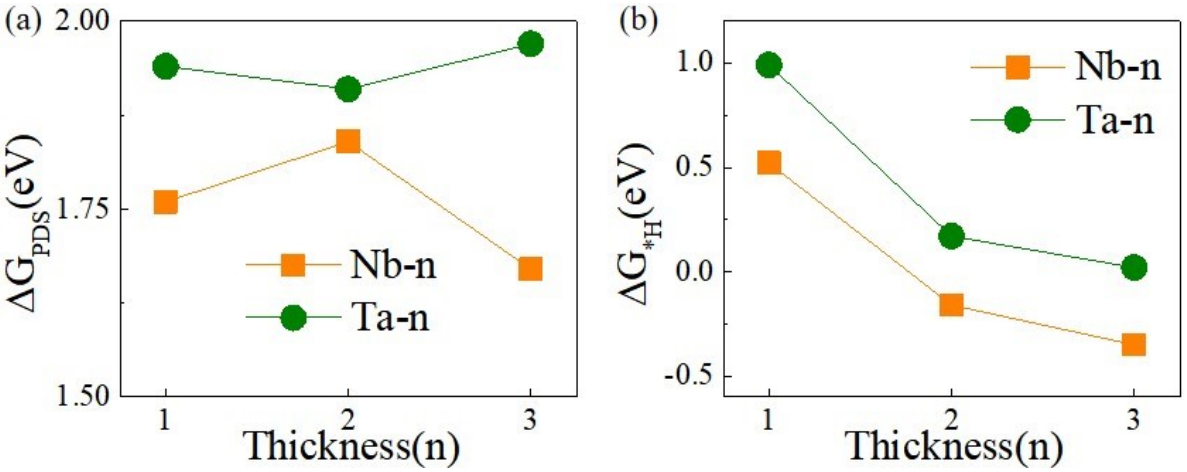

Figure S9: (a) OER and (b) HER for $BaXNO_2$-n (X = Nb, Ta).

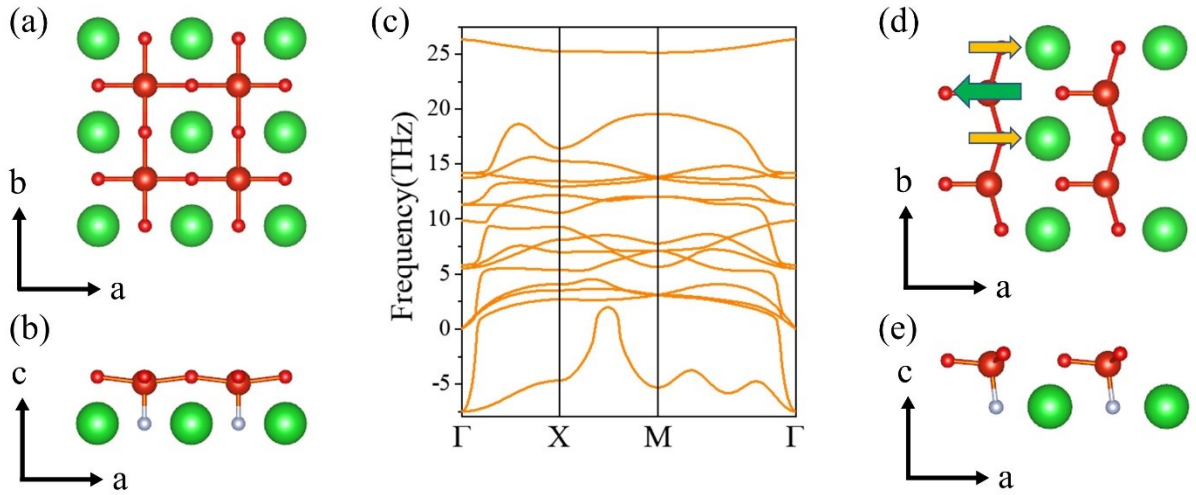

Figure S10: Center-symmetric $BaVNO_2$-1. (a) Top and (b) side views. (c) Phonon dispersion. (d) Top and (e) side views with the in-plane opposite displacements of V and O ions. The direction of the in-plane ferroelectric distortion is marked by green and yellow arrows.

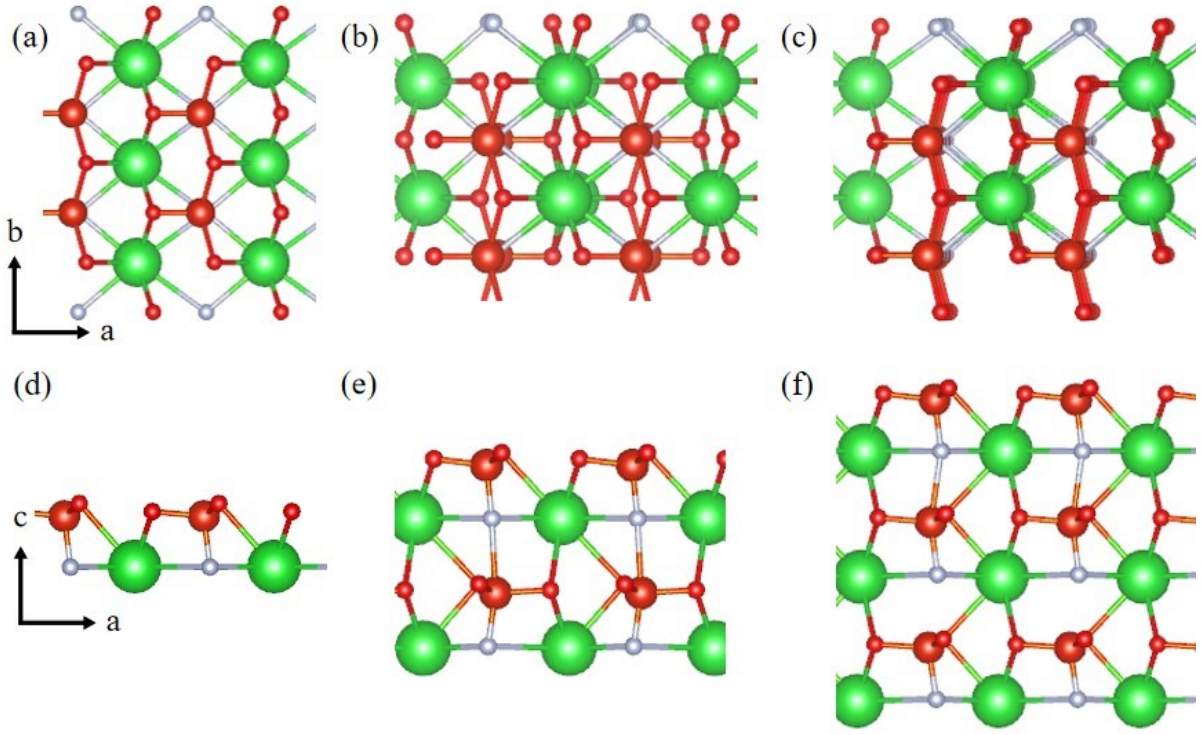

Figure S11: Top views and side views of (a), (d) FE $BaVNO_2$-1, (b), (e) AFE $BaVNO_2$-2, and (c), (f) FE $BaVNO_2$-3.

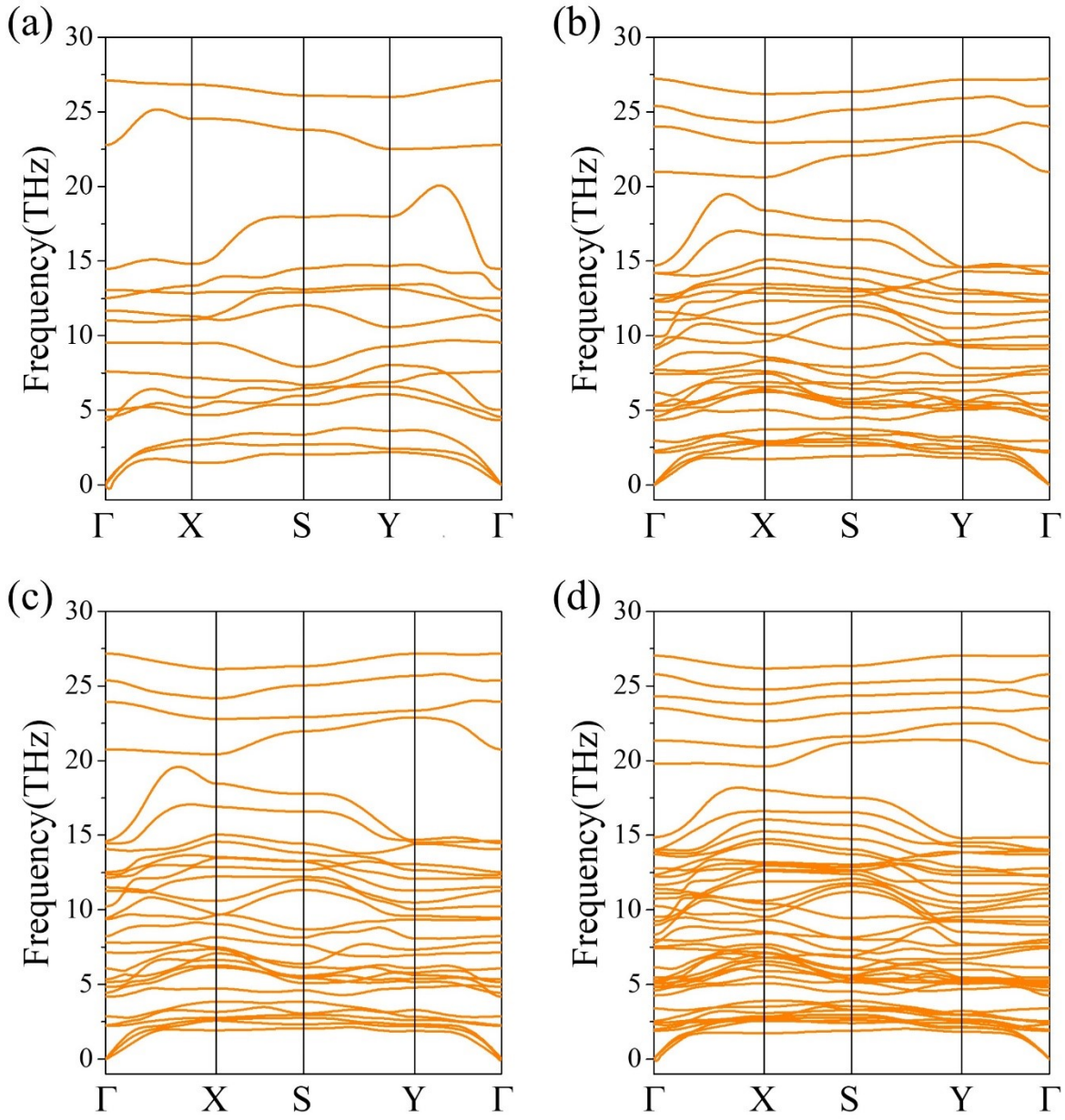

Figure S12: Phonon dispersions of (a) FE $BaVNO_2$-1, (b) FE $BaVNO_2$-2, (c) AFE $BaVNO_2$-2, and (d) FE $BaVNO_2$-3

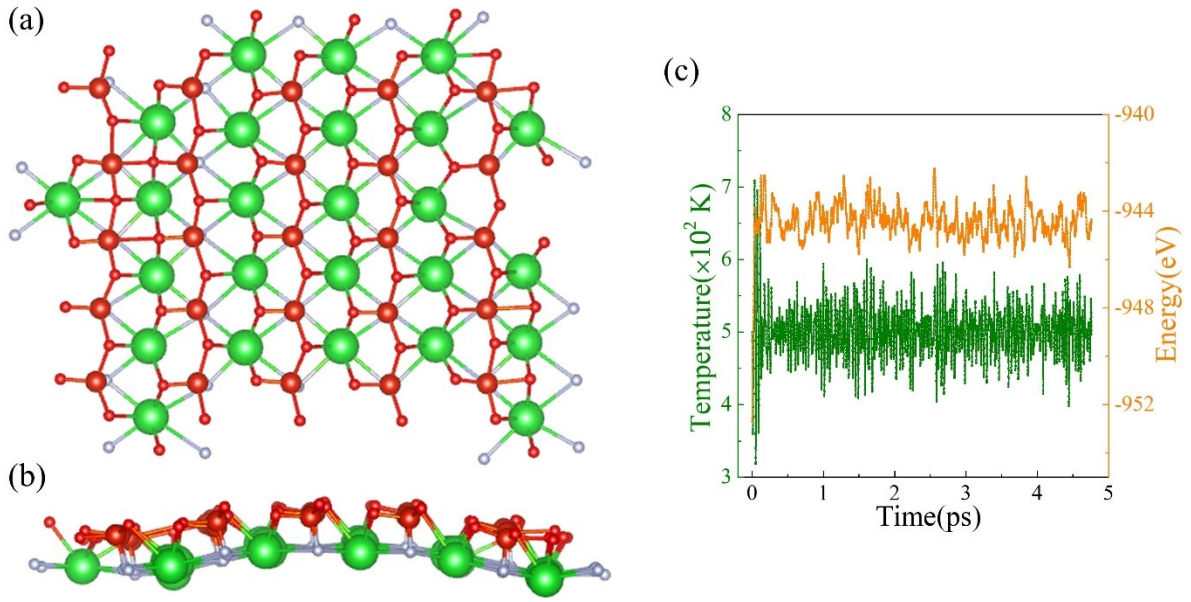

Figure S13: (a) Top and (b) side view of FE $BaVNO_2$-1 after AIMD for ~ 5 ps. (c) Total energy (orange) and temperature (olive) of FE $BaVNO_2$-1 as a function of time.

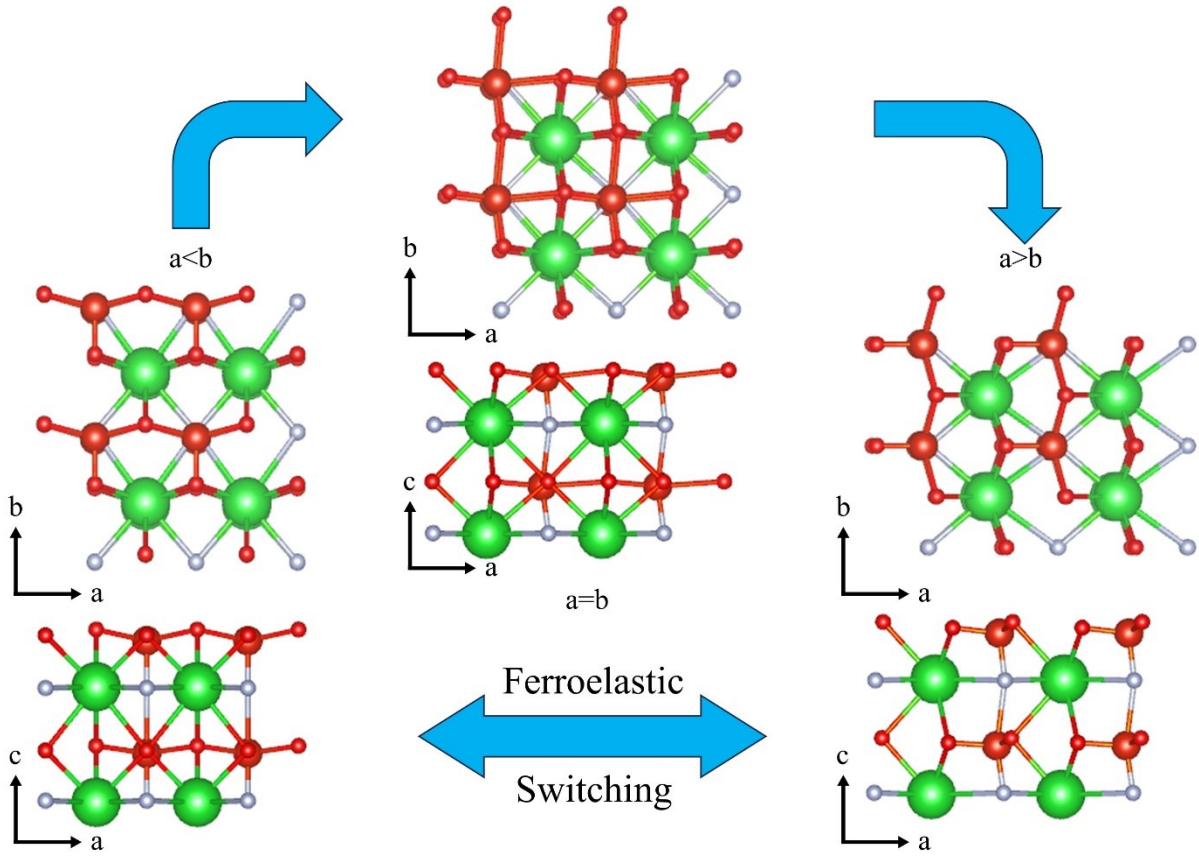

Figure S14: Schematic diagram of ferroelastic switching for FE $BaVNO_2$-2.

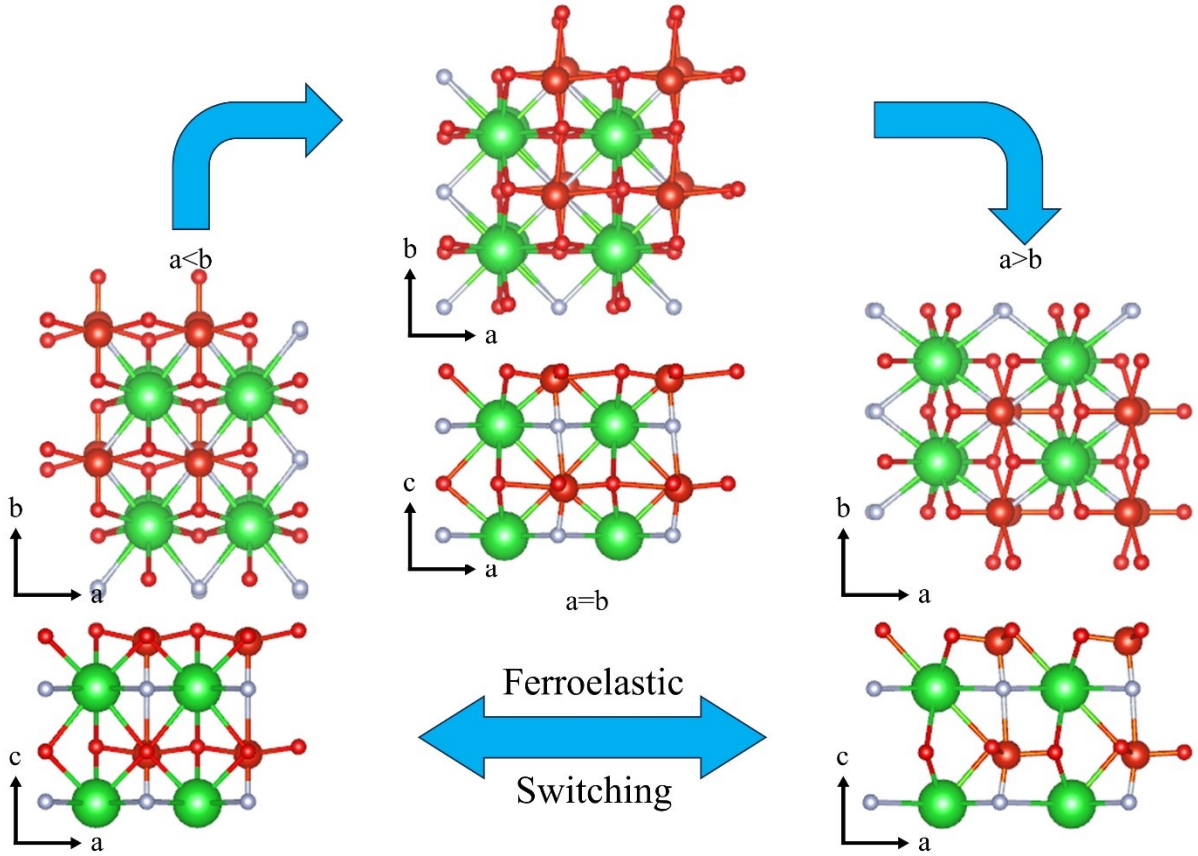

Figure S15: Schematic diagram of ferroelastic switching for AFE $BaVNO_2$-2.

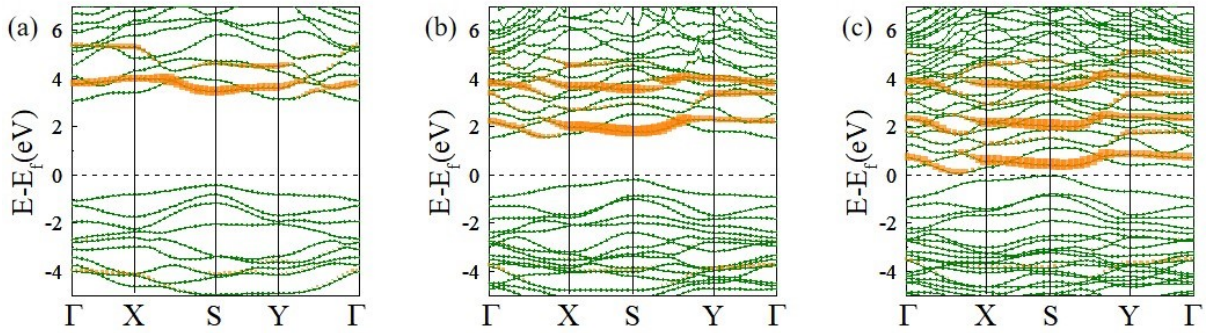

Figure S16: Band structures (olive) and projected band structures (orange) of V-d_{xy} orbitals: (a) FE $BaVNO_2$-1, (b) AFE $BaVNO_2$-2, and (c) FE $BaVNO_2$-3.

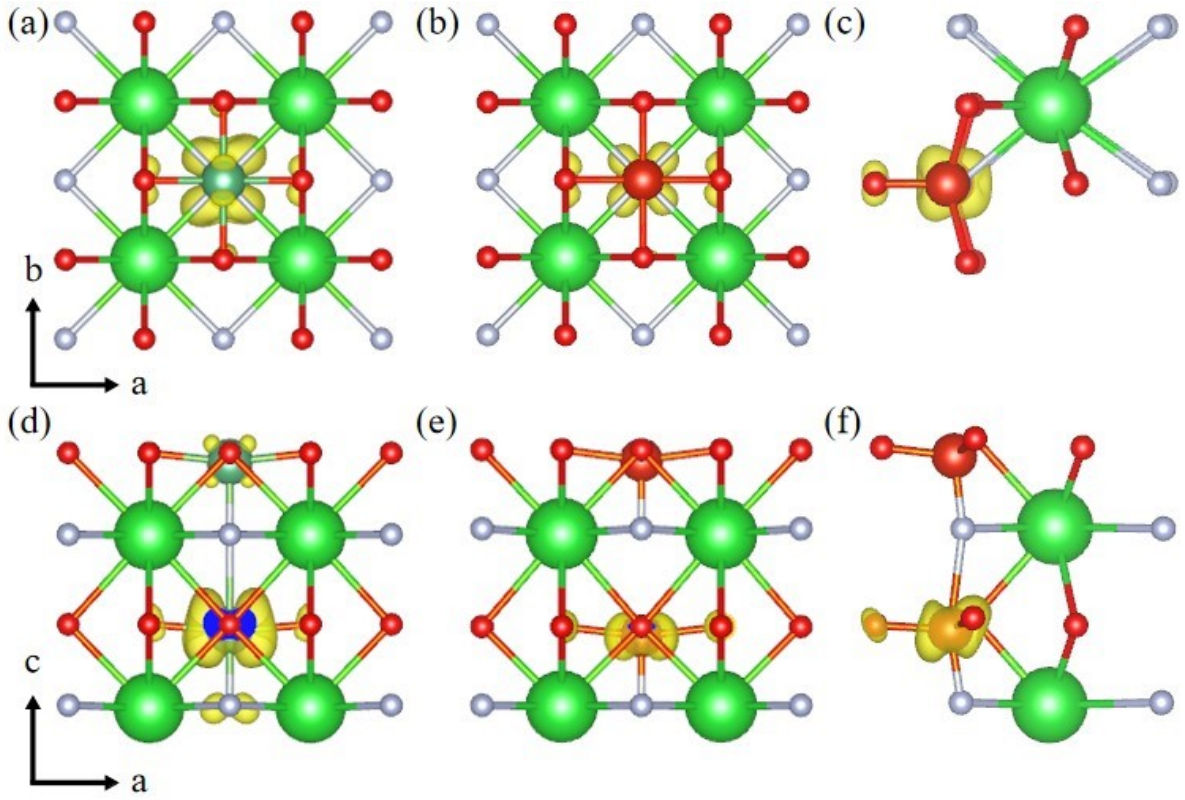

Figure S17: Band decomposed charge density of CBM. Top views and side views: (a), (d) $BaNbNO_2$-2, (b), (e) PE $BaVNO_2$-2, and (c), (f) FE $BaVNO_2$-2.

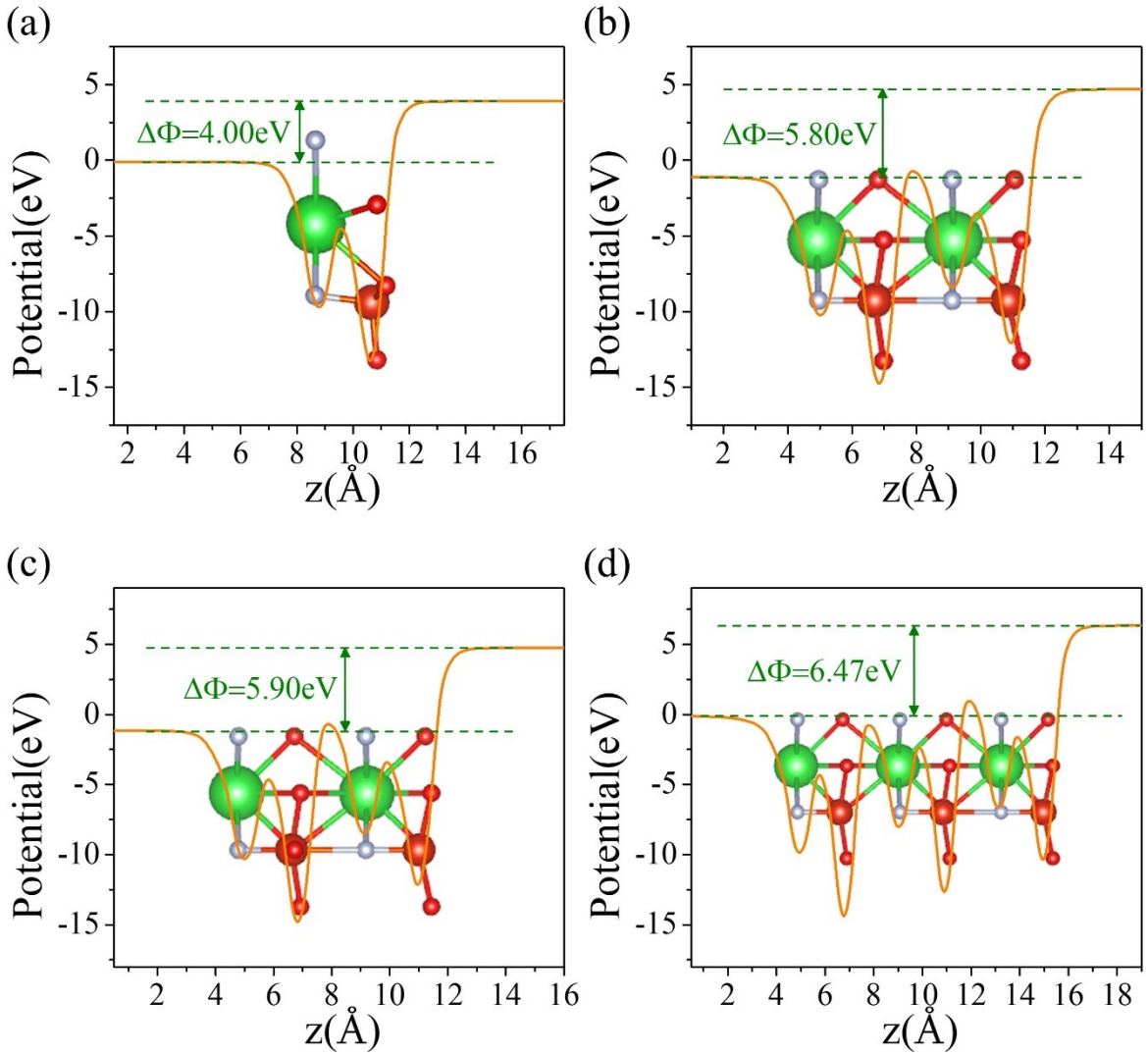

Figure S18: Electrostatic potential of (a) FE $BaVNO_2$-1, (b) FE $BaVNO_2$-2, (c) AFE $BaVNO_2$-2, and (d) FE $BaVNO_2$-3 along the z direction.

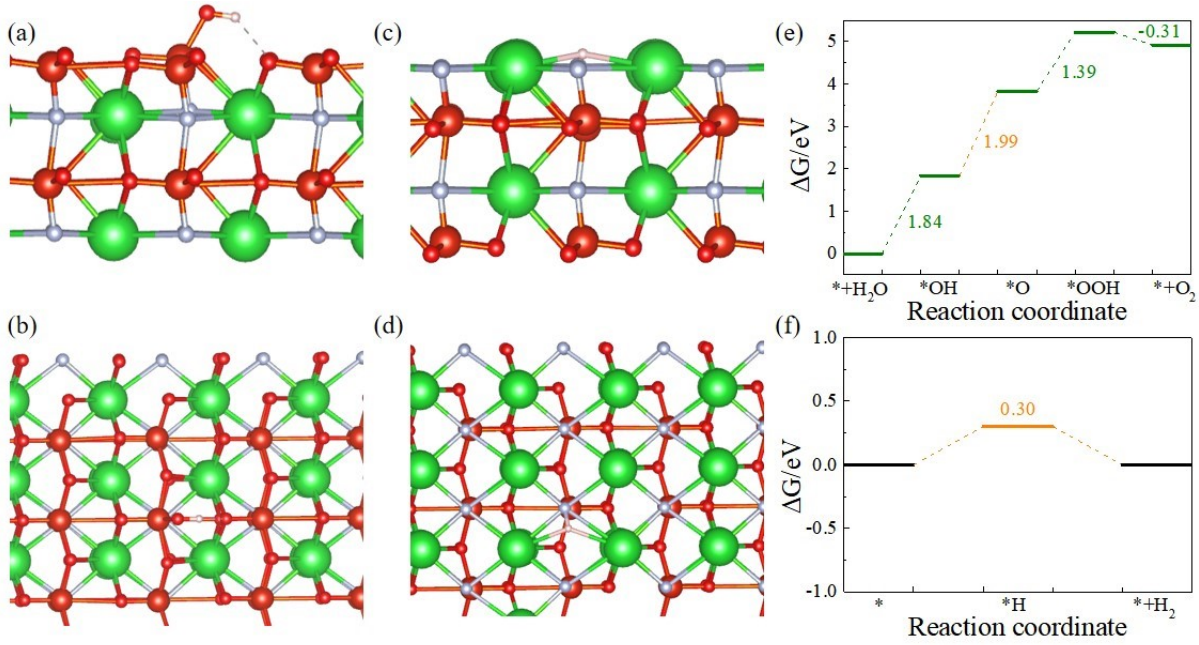

Figure S19: (a) Side view and (b) Top view of $BaVNO_2$-2 with OH adsorbed (*OH). (c) Side view and (d) Top view of $BaVNO_2$-2 absorbing H (*H). Free energy diagrams of (e) OER and (f) HER of FE $BaVNO_2$-2.

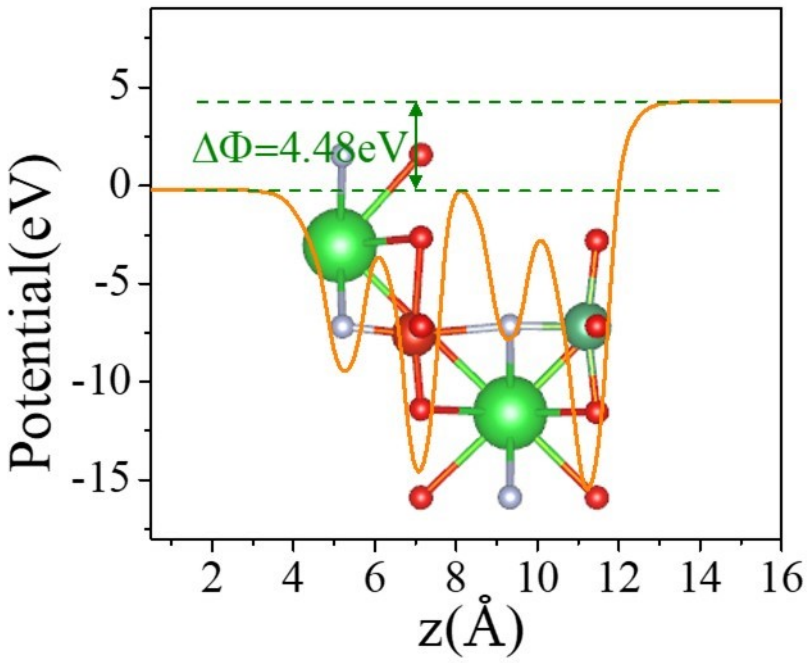

Figure S20: Electrostatic potential of $BaNbNO_2$-1/$BaVNO_2$-1 heterostructure along the z direction.

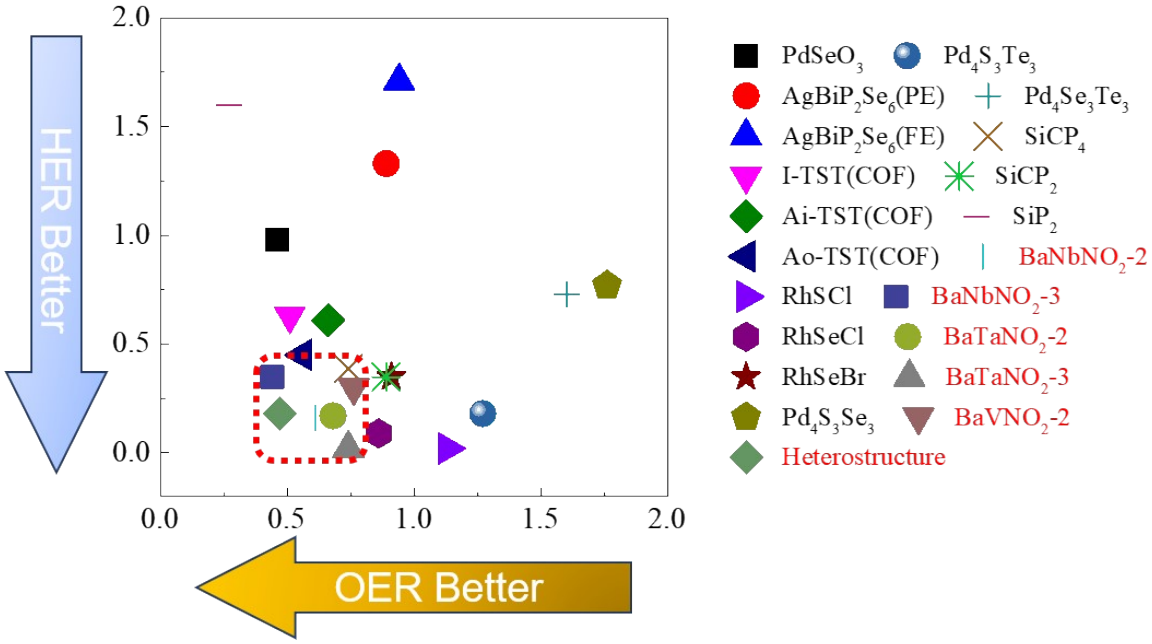

Figure S21: A full comparison of bi-functional activity with the state-of-art photocatalysts for overall water splitting.